Investigating the Sulfur Mystery in Protoplanetary Disks Through Chemical Modeling

Becky J. Williams

Advisor: L. Ilsedore Cleeves

May 10th, 2024

Department of Astronomy

University of Virginia

This thesis is submitted in partial completion of the requirements of the BA Astronomy Major.

Abstract

Sulfur is a critical element to life on Earth, and with detections of sulfur-bearing molecules in exoplanets and comets, questions arise as to how sulfur is incorporated into planets in the first place. In order to understand sulfur's journey, we need to understand the molecular forms that sulfur takes in protoplanetary disks, where the rotational emission from sulfur-bearing molecules in the gas phase indicates a very low abundance. To address this question, we have updated the 2D time-dependent disk chemical modeling framework of Fogel et al. (2011) to incorporate several new sulfur species and hundreds of new sulfur reactions from the literature. Specifically, we investigate the main molecular forms that sulfur takes in a disk orbiting a solar mass young T Tauri star. We explore the effects of different volatile (reactive) sulfur abundances, C/O ratios, and initial sulfur molecular forms. We find that a high C/O ratio can explain both the prevalence of CS observed in disks and the lack of SO detections, consistent with previous results. Additionally, initial sulfur form greatly affects the ice abundances in the lower layers of the disk, which has implications for comet formation and future observations with JWST.

1 Introduction

One of the keys to understanding the emergence of life is understanding the history of life's required elements. Sulfur is one of the elements critical to life on Earth and is thought to play a role in the origin of life. For example, sulfur-bearing molecules in early Earth's atmosphere may have provided protection against harmful solar radiation (Kasting et al. 1989), and evidence suggests that early microbial life metabolized sulfur (Lake 1988).

Sulfur, in the form of SO_2, was recently detected in the atmosphere of exoplanet WASP-39b (Rustamkulov et al. 2023). This detection raises the question of how sulfur is incorporated into planets in the first place. To answer this question, we need to understand the molecular forms and distribution of sulfur in protoplanetary disks.

Protoplanetary disks are disks of gas and dust that surround young stars. Disks are the sites of planet formation, so by studying disks we can bridge the gap between star formation and planetary systems. As described in Williams and Cieza (2011, and references therein), stars form from the collapse of a molecular core, and a disk soon forms around this protostar. For the first ~ 0.5 Myr, the disk is considered protostellar, meaning much of the material in the disk will end up accreting onto the star. The disk then transitions to protoplanetary. Disks have masses of about 1% the mass of their stars and are about 30-200 au in extent, with the densest (and coldest) regions at the midplane. They are about 1% dust and 99% gas by mass. Disk lifetimes range from < 1 Myr to 10 Myr, with a median of about 3 Myr (Strom et al. 1989; Wyatt 2008; Mamajek 2009).

Broadly, disks are classified as T Tauri or Herbig disks. T Tauri stars are spectral types F, G, K, and M, so they are most similar to our own solar system, making them exciting for understanding our solar system's past. Herbig stars are spectral types A and B (i.e., more massive than our Sun), and their disks are typically more massive.

Protoplanetary disks are interesting for many reasons, including that they are astrochemically fascinating objects. So far, 25 unique molecules have been detected in disks (McGuire 2022), the most abundant (after H_2) being CO. With telescopes like ALMA, it is possible to detect, and spatially resolve, molecules in these disks. These molecular detections are important for understanding what molecules are present to potential forming planetesimals and for inferring the chemical and physical structures and conditions of disks.

Disks consist of three main chemical layers, described in detail in Bergin and Cleeves (2018). The disk midplane is the coldest, densest region, dominated by ices. Moving vertically upward, the warm molecular layer is the zone of gas-phase molecules, defined by where the dust temperature exceeds the sublimation temperature of CO (Aikawa et al. 2002). In the highest layers of the disk, molecules are dissociated in a region called the atomic-to-molecular transition.

One of the main goals of studying disk chemistry is accounting for the budget of the most abundant elements in the Universe, such as carbon, oxygen, and sulfur. From

studying the Sun, we know the total expected abundances of the elements relative to hydrogen (Asplund et al. 2021). Some fraction of these elements is locked up in dust in the disk, while the remaining fraction is volatile, meaning it can react and form molecules. Carbon primarily resides in CO, but several other forms of carbon, including more complex species like CH_3OH and CH_3CN, have been detected in disks (McGuire 2022; Walsh et al. 2016; Öberg et al. 2015). Oxygen is a current mystery, as its two main carriers, CO and H_2O, are detected in low abundance in disks, and no other molecules have been detected in high enough abundance to account for the remaining budget (e.g. Dutrey et al. 1994; Ansdell et al. 2016; Long et al. 2017; Du et al. 2017; Williams et al. 2023). Sulfur, the focus of our work here, is another mystery, observed in low abundance relative to its solar abundance.

The solar sulfur abundance relative to hydrogen is 1.4×10^{-5} (Asplund et al. 2021). In protoplanetary disks, the majority of sulfur is predicted to be in refractory form. Using observations of stellar photospheres, Kama et al. (2019) measured that $\approx 89 \pm 8\%$ of sulfur is in a non-observable and non-reactive refractory form such as FeS.

Several gas-phase sulfur-bearing molecules have been detected in low abundance in disks. The most widely detected is CS, which has been observed in several disks, including IM Lup, GM Aur, AS 209, HD 163296, MWC 480, and TW Hya (Le Gal et al. 2021; Teague et al. 2018). Other gas-phase molecules that have been detected in disks include SO, H_2S, H_2CS, and SO_2. Phuong et al. (2021) detected C_2S in the protoplanetary disk GG Tau.

Semenov et al. (2018) searched for CS, SO, SO_2, OCS, C_2S, H_2CS, and H_2S in DM Tau, and only detected CS, and tentatively SO_2. They suggest that a C/O ratio $\gtrsim 1$ is needed to explain the inferred high abundance of CS relative to other species, specifically SO and SO_2. This observation is likely linked to the depletion of oxygen observed in disks. Modeling by Le Gal et al. (2021) and Keyte et al. (2023) has shown that the C/O ratio has a large effect on the resulting abundances of sulfur-bearing species, including the CS/SO ratio.

CS, SO, and H_2S have all been detected in AB Auriga, a Herbig Ae star (Fuente et al. 2010; Rivière-Marichalar et al. 2022), whose disk has an asymmetric continuum. Abundances of these molecules are on the order of 10^{-11} relative to hydrogen.

A number of sulfur detections are linked to unique morphologies and processes. Law et al. (2023) detected SO and SiS in HD 169142, likely tracing outflow from a young planet. Booth et al. (2021) detected SO and SO_2 in Oph-IRS 48, a Herbig source that has a dust trap. Both SO and SO_2 emission spatially coincide with the location of the dust trap, while CO emission covers the full azimuth extent of the disk. Booth et al. (2021) calculate a detected S/H ratio of $4.6 - 10.0 \times 10^{-7}$, which accounts for $\approx 15 - 100\%$ (compared to solar) of the total volatile sulfur budget. They propose that SO and SO_2 form in the ice-phase in the dust trap and then sublimate, causing these high abundances. In contrast to observations of other disks, they do not detect CS in Oph-IRS 48, and therefore calculate a very low CS/SO < 0.01.

Keyte et al. (2024) studied the disk HD 100546, using ALMA and APEX observations, as well as chemical modeling, to determine that the volatile S/H $\sim 10^{-8}$, and predict that the main gas-phase carriers are OCS, H_2CS, and CS. They also predict a substantial OCS ice reservoir.

While observations of disks have yielded several detections of sulfur-bearing molecules, the vast majority of sulfur remains undetected in protoplanetary disks, and several questions remain as to the evolution and abundance of sulfur through the protoplanetary disk phase. To probe at this hidden reservoir, we updated our existing reaction network and used 2D chemical modeling and a variety of initial conditions.

2   Methods

To explore the sulfur chemistry of protoplanetary disks, we use a 2D disk chemical code, updated to include more sulfur species and reactions. This code allows us to model the abundances of molecular species over time for all points in a disk. Table 1 lists the parameters of each run, along with our naming convention for each run. We explore a range of volatile sulfur abundances, C/O ratios, and initial sulfur molecular form to investigate how these parameters affect the sulfur chemistry. We varied the abundance of total volatile sulfur from 1×10^{-9} to 1×10^{-7}. For the mid-sulfur case (1×10^{-8}), we varied the initial sulfur form (CS and SO, H_2S, S_8 ice, S). We also explored the effect of the C/O ratio (C/O = 0.36, 0.85, and 1.40) by reducing the abundance of volatile oxygen. The C/O ratio has previously been shown to have a large effect on the CS/SO ratio in disks (Le Gal et al. 2021; Keyte et al. 2023).

Table 1: 2D Model Runs.

Run	S Abundance	Initial Form	C/O Ratio
low1	1×10^{-9}	CS & SO	0.36
low2	1×10^{-9}	CS & SO	0.85
low3	1×10^{-9}	CS & SO	1.40
mid1	1×10^{-8}	CS & SO	0.36
mid2	1×10^{-8}	CS & SO	0.85
mid3	1×10^{-8}	CS & SO	1.40
mid4	1×10^{-8}	H_2S	0.36
mid5	1×10^{-8}	S_8 ice	0.36
mid6	1×10^{-8}	S	0.36
high1	1×10^{-7}	CS & SO	0.36
high2	1×10^{-7}	CS & SO	0.85
high3	1×10^{-7}	CS & SO	1.40

2.1 Chemical Model

We are using the chemical model of Fogel et al. (2011), which has since been updated (Anderson et al. 2021). We initially explored the disk chemistry using a 1D chemical model before incorporating our updated network into a 2D chemical model, which we will be focusing on for the remainder of this paper. The 2D model is a time dependent, radius independent model. We run the model up to 1 Myr, with 60 log-spaced time steps, and we analyze the output at 1 Myr.

2.2 Reaction Network

2.2.1 Original Network

The original network contained 645 species and 6163 reactions. It first came from Fogel et al. (2011), based on the Ohio State University gas-phase model from Smith et al. (2004), though it has since been updated (Anderson et al. 2021, and references therein).

Reactions include gas-phase reactions, grain-surface reactions, photoreactions, cosmic ray ionization, x-ray induced UV photolysis, and x-ray ionization of H_2 and He. Every molecular species has an adsorption, a desorption, a photodesorption, and a cosmic ray desorption reaction. The network also includes self-shielding of CO, H_2, and N_2.

2.2.2 Updated Network

We update our existing reaction network with the new reactions presented in Laas and Caselli (2019). Laas and Caselli (2019) investigated the sulfur chemistry of interstellar clouds, and the majority of these new reactions involve sulfur-bearing molecules. These reactions include several gas-phase reactions, grain surface reactions, photoreactions, and cosmic ray ionization. For every species, we also added reactions for adsorption, desorption, photodesorption, and cosmic ray desorption. The updated network includes 707 species and 6825 reactions.

After updating our network, we confirmed that no reactions were repeated, all reactions conserved charge and mass, and every molecular species had a destruction and production reaction. We also compared the output of our new network with that of the original network to confirm that key species like CO and H_2O were minimally affected by the changes.

2.3 Binding Energy

We added several new sulfur species to our network. When adding binding energies for these species, we defaulted to using the binding energies from Laas and Caselli (2019). The exception is for the sulfur allotropes (S_2 through S_8), where we used the binding energies from Cazaux et al. (2022), though we note that there is a range

of sulfur allotrope binding energies in the literature (e.g., Laas and Caselli 2019; Ligterink and Minissale 2023). Lastly, for species that were already present in our network, the only binding energies that we updated were for the carbon-sulfur chains (i.e., C_xS_y) (Laas and Caselli 2019).

2.4   Disk Physical Structure

Our disk physical conditions come from the 2D disk model presented in Gross et al. (2024, in prep), which is based on Anderson et al. (2021). We use the fiducial model, where the disk is azimuthally symmetric and has a radius of 120 au and a disk mass of 0.01 $M_\odot$. At the center of the disk is a 1 $M_\odot$ T Tauri star (radius = 2.8 $R_\odot$, effective temperature = 4300 K).

The dust temperatures assume passive heating by the star and are calculated using TORUS (Harries et al. 2004). The dust consists of two populations, a large and a small dust population, both of which have a minimum dust size of 0.005 μm. The large population, comprising 90% of the total dust mass, has a maximum size of 1 mm. The small population has a maximum size of 1 μm and contains the remaining 10% of dust mass.

The UV radiation field uses the spectrum from TW Hya, and the X-ray radiation field assumes a total X-ray luminosity of $10^{29.5}$ erg s^{-1} between 1 and 20 keV. These inputs are used in a Monte Carlo radiative transfer code (Bethell and Bergin 2011a,b). Gas temperatures come from the local UV flux and gas density, using the models from Bruderer (2013) as in Cleeves et al. (2015). The cosmic-ray ionization comes from Cleeves et al. (2015), with an incident rate of 1.1×10^{-18} s^{-1} on the surface of the disk.

3   Results

The results of the 2D model runs, using varying initial condition parameters, are presented below. For the names of model runs, refer to Table 1.

3.1   Standard Case

We refer to the standard case (mid1) as the run where S/H = 1×10^{-8}, C/O= 0.36, and initially sulfur is in gas-phase CS and SO. We use this as our base case for comparison to other model runs. The abundances of fifteen sulfur species are shown in Figure 1.

3.2   Effects of Volatile Sulfur Abundance

We varied the volatile sulfur abundance from 1×10^{-9} to 1×10^{-7}. Figure 2 shows the enhancements in CS and SO as the volatile abundance is increased. We compare
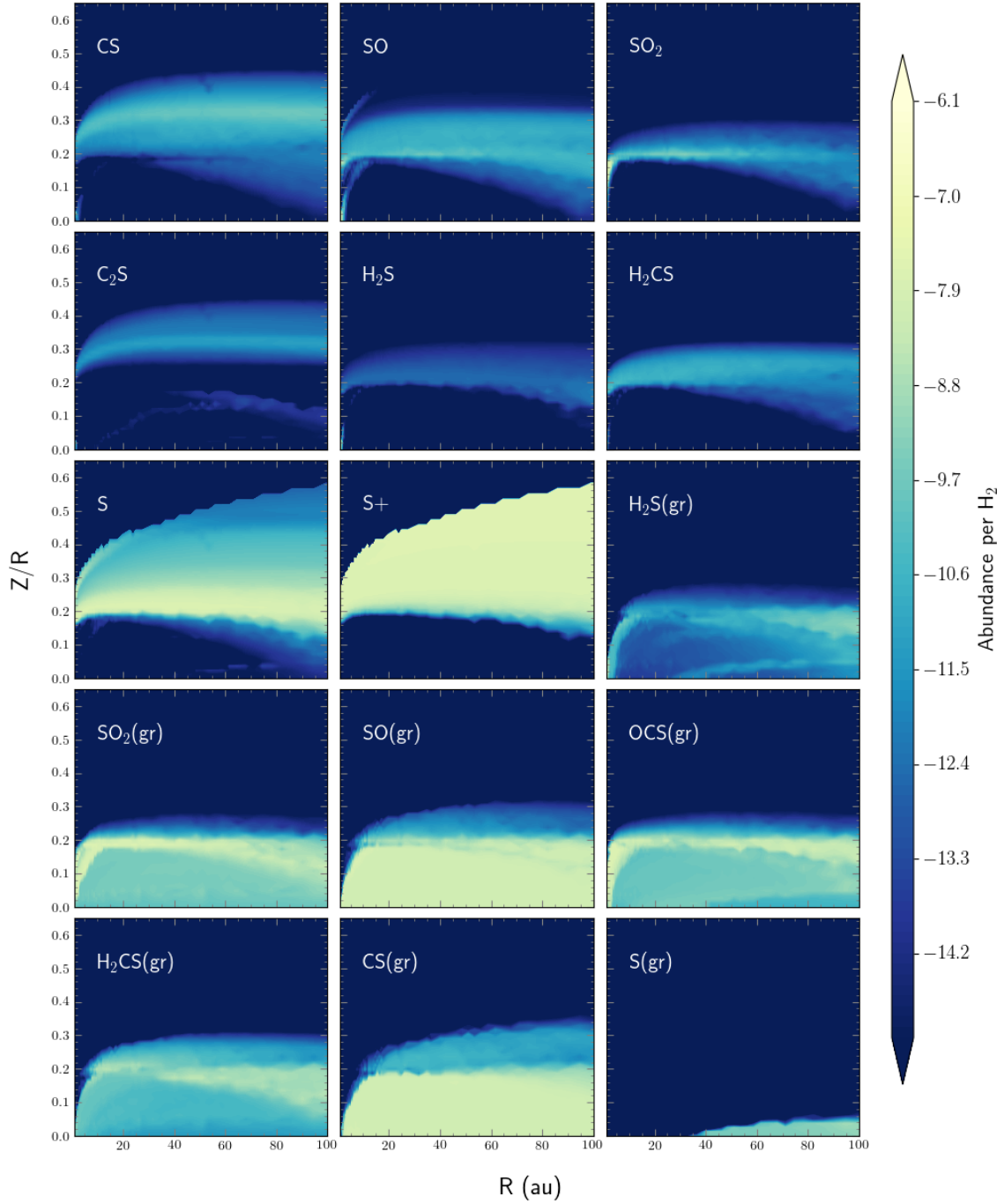
Figure 1: Abundances of 15 sulfur-bearing species in a generic disk for the standard case (mid1). The total sulfur abundance is $S/H_2 = 2 \times 10^{-8}$, $C/O = 0.36$, and the initial sulfur form is gas-phase CS and SO.

the mid case to the low case, and the high case to the mid case. In the mid case, CS and SO are roughly an order of magnitude higher in abundance throughout the disk, relative to the low case. In the high case, the enhancement is heterogeneous, with the region around $Z/R = 0.2$ varying from a uniform increase. CS is enhanced in abundance by less than an order of magnitude, while SO increases in abundance by more than an order of magnitude.

3.3   Effects of C/O Ratio

For each abundance case, we explored the effects of a C/O ratio of 0.36, 0.85, and 1.40. The C/O ratio was altered by depleting oxygen from H_2O ice and CO. Here, we consider the mid sulfur case, though we note that the low and high sulfur cases had similar results. Figure 3 shows the CS and SO abundances in the 0.85 and 1.40 cases, relative to the 0.36 case. At $C/O = 1.40$, CS is up to 4 orders of magnitude more abundant than in the $C/O = 0.36$ case, and SO is up to 4 orders of magnitude less abundant. Interestingly, in the $C/O = 0.85$ case, both CS and SO show slight enhancements relative to the $C/O = 0.36$ case.

3.4   Effects of Initial Sulfur Form

For most of our models, we started the sulfur in gas-phase CS and SO. For the mid sulfur case, we also ran models with the sulfur starting in H_2S, S_8 ice, and S. In all three cases, the gas-phase abundances (above $Z/R \approx 0.2$) remain roughly the same, while the ice-phase abundances reflect the initial sulfur form. The one exception is the case where the sulfur begins as atomic S; in this case, the main sulfur form in the ice phase is OCS ice. The abundances of several ice species, compared between these four models, are shown in Figure 4.

4   Discussion

Here, we consider in more depth the results and their implications. We consider the effects in the warm upper layers of the disk ($Z/R = 0.2 - 0.4$), where gas-phase molecules dominate, and in the cold lower layers of the disk ($Z/R \leq 0.2$), where ices dominate. Above $Z/R \sim 0.4$, gas-phase molecules do not survive and S^+ dominates.

4.1   Upper Layer ($Z/R = 0.2 - 0.4$)

In the warm upper layers of the disk ($z/r \approx 0.2$-0.4), we find the majority of sulfur in gas-phase molecules. The abundance of CS peaks at $Z/R \approx 0.3$, while SO peaks at $Z/R \approx 0.2$. Initial sulfur form does not have a noticeable effect on the abundances of the gas-phase sulfur species in this region. Due to the warm temperatures and high radiation field, initial complex molecules are soon destroyed.
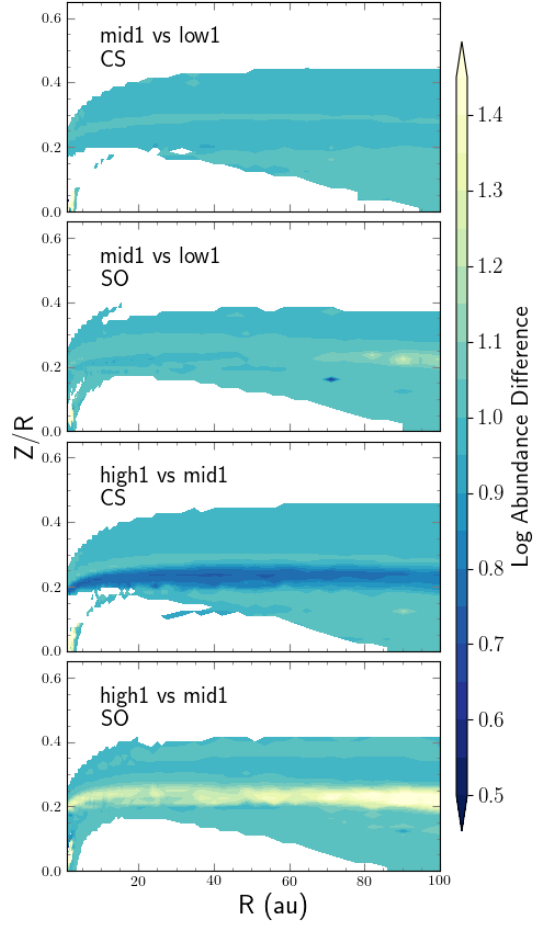
Figure 2: Variations in the abundance of CS and SO for different volatile sulfur abundances. The first two plots compare mid1 to low1 ($S/H = 1 \times 10^{-8}$ to 1×10^{-9}), and the second two plots compare high1 to mid1 ($S/H = 1 \times 10^{-7}$ to 1×10^{-8}). We only plot regions where the abundance of the shown molecule is greater than 1×10^{-15} relative to H_2.
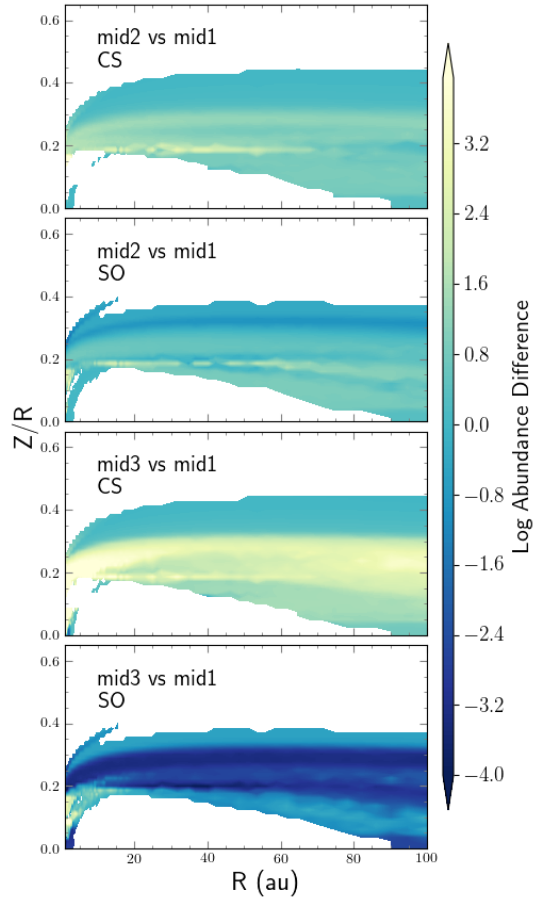
9

Figure 3: Variations in the abundance of CS and SO for different C/O ratios. The first two plots compare mid2 to mid1 (C/O = 0.85 to C/O = 0.36), and the second two plots compare high1 to mid1 (C/O = 1.40 to C/O = 0.85). We only plot regions where the abundance of the shown molecule is greater than 1×10^{-15} relative to H_2.
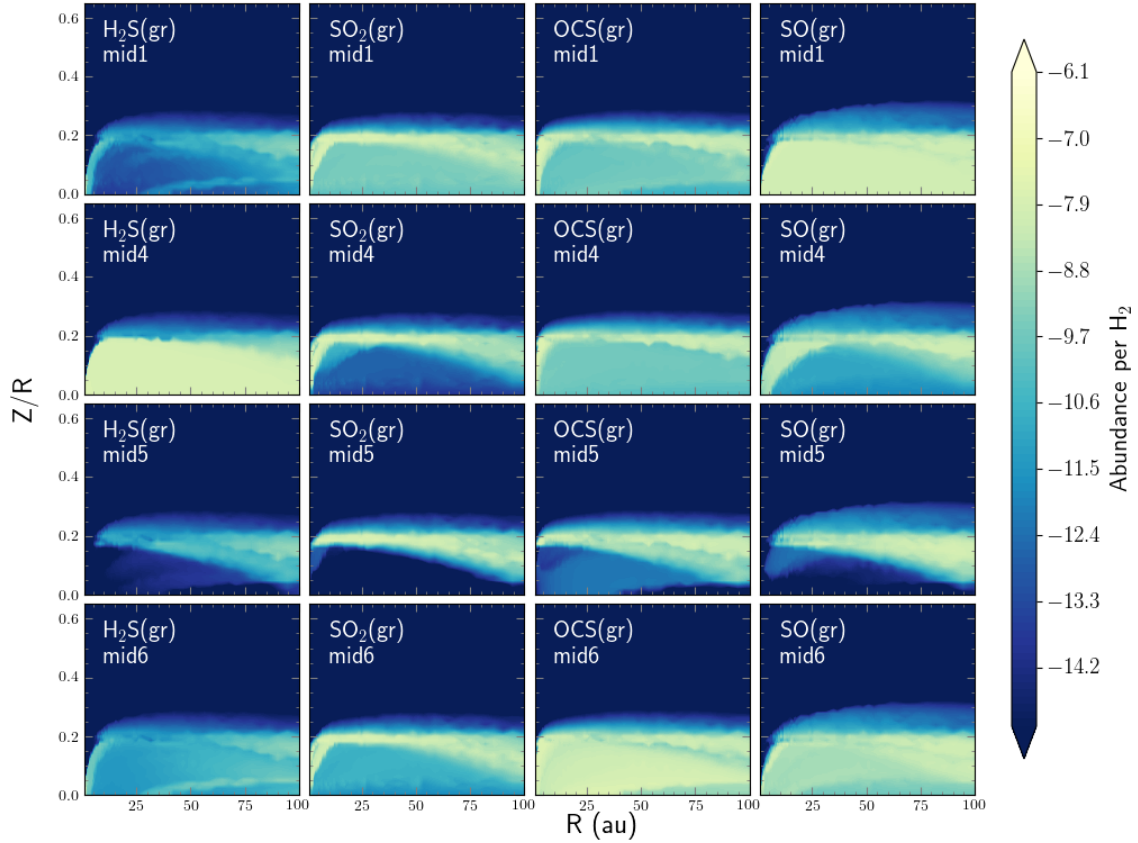
Figure 4: Abundances of four ice species, H$_2$S, SO$_2$, OCS, and SO, for the four models where we varied the initial sulfur form (mid1 in CS and SO, mid4 in H$_2$S, mid5 in S$_8$ ice, and mid6 in S). For more specifics on the model runs, refer to Table 1.

4.1.1 Column Densities

Le Gal et al. (2021) reported the observed column densities of CS in 10 disks (8 T Tauri and 2 Herbig Ae stars), which varies from $0.2 - 6.0 \times 10^{13}$ cm^{-2}, as well as upper limits on SO and C$_2$S for 5 of these disks. Figure 5 shows our disk-averaged column densities of CS, SO, and C$_2$S for all model runs (refer to Table 1 for run parameters). In Figure 5a, the average is calculated from 1 au to 100 au. In Figure 5b, the average is calculated from a radius of 10 au to 100 au. We also show the values from Le Gal et al. (2021) for comparison.

The motivation for excluding the inner 10 au from Figure 5b is that our models show a high abundance in column density of both CS and SO within 10 au of the star (see Appendix), which skews the average. Observations of CS in disks do not show a spike in column density close to the star, and in many cases there is a decrease in CS emission at small radii, resulting in an annulus of emission Le Gal et al. (2021); Teague et al. (2018). The column density of our models is an ideal case that assumes we observe a molecule in all locations of a disk at once. In reality, variations in temperature affect the transition lines that we can observe for a given molecule, and optically thick dust can obscure emission from parts of the disk. For our discussion, we focus on Figure 5b.

We find that increasing the C/O ratio has a large effect on gas-phase abundances (increasing CS and C$_2$S and decreasing SO), consistent with past models and observations Le Gal et al. (2021); Keyte et al. (2023, 2024). While the C/O ratio only varies by a factor of ≈ 4 (from 0.36 to 1.40), the column density of CS increases by more than two orders of magnitude and that of SO decreases by over two orders of magnitude. This trend remains the same for all volatile sulfur abundance cases that we tried (low, mid, and high). We also see that initial sulfur form (mid4, mid5, mid6) has a negligible effect on the column densities of CS, SO and C$_2$S.

The prevalence of CS observed in disks, and lack of SO detections, suggests that CS is in higher abundance than SO (Le Gal et al. 2021). The only models in which CS has a higher column density than SO are the models with C/O = 1.40, and the S/H = 1×10^{-8} case best matches the column densities reported in (Le Gal et al. 2021). There is a large change in abundances from C/O = 0.85 to C/O = 1.4, so it is also likely that an intermediate C/O ratio would best match observations. If we include the inner 10 au in our average, then our results support an intermediary case between S/H = $1 \times 10^{-9} - 10^{-8}$, and a C/O ratio of 1.40. These results are consistent with a large fraction of sulfur being in refractory form (Kama et al. 2019). Keyte et al. (2024) found through modeling of observations that S/H $\sim 10^{-8}$, in agreement with our findings.

A high C/O ratio suggests that volatile oxygen is depleted in disks, leading to a lack of oxygen available for gas-phase molecules. Previous observations of disks have shown that volatile oxygen is in low abundance (e.g. Dutrey et al. 1994; Ansdell et al. 2016; Long et al. 2017; Du et al. 2017), raising questions as to how oxygen can be depleted from the volatile reservoir. One mechanism through which this depletion
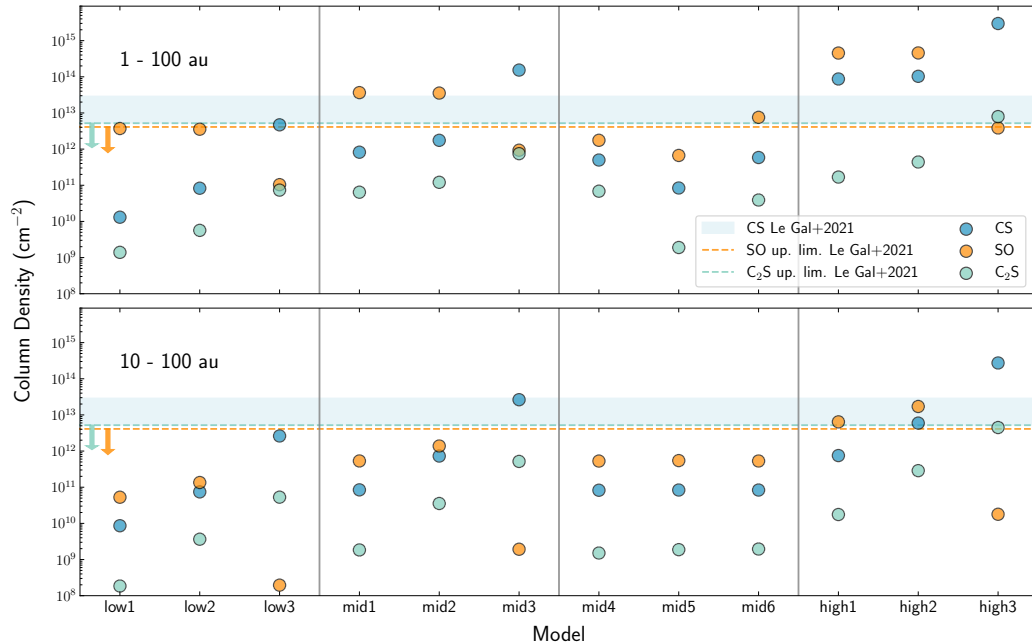
Figure 5: Disk-averaged column densities of CS, SO, and SO$_2$ in our models. The blue shaded region shows detected CS column densities, and the dashed orange and mint green lines show the upper limit range of SO and C$_2$S, respectively, all from Le Gal et al. (2021). The top plot is the average from 1 - 100 au, and the bottom plot is the average from 10 - 100 au. Model runs are listed in Table 1.

can occur is through H$_2$O freezing on dust grains and then settling to the midplane, where the oxygen remains trapped as ice (Hogerheijde et al. 2011; Bergin et al. 2016; Du et al. 2017). This mechanism would result in a high C/O ratio in the upper layers of the disk and low C/O ratio in the lower layers of the disk, where the H$_2$O settles. We note that our models do not take into account this settling mechanism, as there is no vertical transport of matter in our models. However, given that our models show that molecular sulfur probes intermediate vertical heights, we can interpret our model results as pointing to an elevated C/O ratio in the upper disk layers.

4.1.2 Gas-phase Observations

The most abundant gas-phase species in our models vary slightly with C/O ratio. Table 2 lists the most abundant sulfur-bearing species at 40 au, for a Z/R = $0.0, 0.1, 0.2, 0.3$, and 0.4, as the C/O ratio increases. Note that, as explained in Section 4.1.1, a high C/O ratio is unlikely in the midplane, but we include the results in the midplane for completeness. At high Z/R, S$^+$ and S are the main carriers.

Focusing on Z/R = 0.3, as the C/O ratio increases, SO and HS are replaced by the carbon sulfur chains C_2S and C_3S as some of the main carriers. Based on our model output, after CS, C_2S should be the most abundant sulfur molecule detected in disks. Looking at Figure 5, in the mid3 case, C_2S is just shy of the upper limits on observations from Le Gal et al. (2021). Future deep observations targeting C_2S would provide observational support that a high C/O ratio is present in the upper layers of disks.

Table 2: Most Abundant Sulfur Species at 40 au.

Z/R	mid1 (C/O = 0.36)	mid2 (C/O = 0.85)	mid3 (C/O = 1.40)
0.0	CS(gr), SO(gr), OCS(gr), C_3S(gr), S(gr)	CS(gr), SO(gr), OCS(gr), C_3S(gr), S(gr)	CS(gr), S(gr), OCS(gr), C_2S(gr), SO(gr)
0.1	CS(gr), SO(gr), C_3S(gr), SO_2(gr), OCS(gr)	CS(gr), SO(gr), C_3S(gr), SO_2(gr), OCS(gr)	CS(gr), HNCS(gr), SO(gr), C_3S(gr), HCS(gr)
0.2	S, SO_2(gr), OCS(gr), SO(gr), S^+	S, H_2CS(gr), OCS(gr), S^+, CS(gr)	CS(gr), H_2CS(gr), HCS(gr), NS(gr), HS(gr)
0.3	S^+, S, CS, SO, HS	S^+, S, CS, C_2S, C_3S	S, CS, S^+, C_2S, C_3S
0.4	S^+, S, CS, C_2S, SO^+	S^+, S, CS, C_2S, SO^+	S^+, S, CS, C_2S, SO^+

4.2 Lower Layer (Z/R ≤ 0.2)

Lower in the disk, where temperatures are colder, initial sulfur form plays a big role. In the three molecular cases we tried (initial sulfur as gas-phase CS and SO, as gas-phase H_2S, or as S_8 ice), the main sulfur carriers at low Z/R were the ice-phase versions of the initial carriers. When sulfur started as atomic S, the main carrier was OCS ice, followed by S ice. These result suggests that initial sulfur form in a protoplanetary disk will largely determine the ices available for comet and planet formation, as sulfur molecules are minimally processed in the midplane in our models.

4.2.1 Allotropes

Sulfur is capable of forming large sulfur chains, S_2 through S_8, and one possible hiding spot for sulfur is in these large, stable, allotropes. In our models, there is no build-up
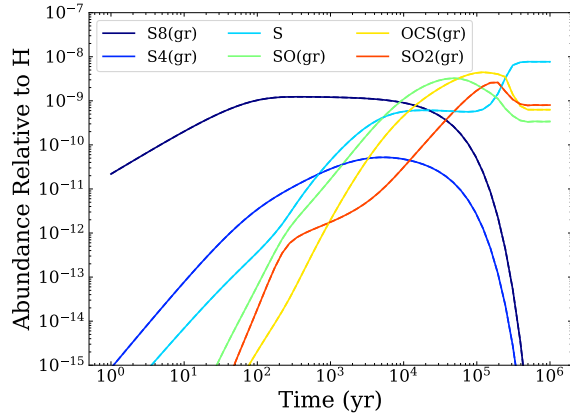
Figure 6: Abundance of sulfur species over time at R = 40 au, Z = 8 au (Z/R = 0.2), for run mid5, where sulfur begins in the form S_8 ice. Sulfur allotropes are destroyed around $10^4 - 10^5$ yr, as simpler sulfur molecules (S, SO_2 ice, OCS ice, and SO ice) become the dominant sulfur carriers.

of S_3 or higher, in disagreement with this hypothesis. The only model in which we see significant amounts of allotropes is when sulfur begins as S_8 ice, where it remains in that form in the lower layers of the disk, but is broken apart in the upper layers. Figure 6 shows the abundance of several sulfur molecules over time at R = 40 au, Z = 8 au (Z/R = 0.2), which has a gas and dust temperature of 47 K. S_8 ice declines sharply at about 5×10^4 yr. S_8 ice is broken down by photons into smaller sulfur allotrope ices, which are further broken down into S ice. S ice thermally desorbs from the grain and is then available for gas-phase reactions.

Our models suggest that S_8 is not a main carrier of sulfur, unless sulfur begins in that form. Laas and Caselli (2019), which we updated our network based on, also did not find significant build-up of allotropes in their molecular cloud models. More recently, Shingledecker et al. (2020) incorporated cosmic-ray-driven radiation chemistry and nondiffusive bulk reactions into their dense molecular cloud models. They also based their network on the one from Laas and Caselli (2019), and by incorporating these two additional processes, they found a significant buildup of sulfur allotropes, along with OCS and SO_2 ices. If sulfur allotropes do indeed form in dense molecular clouds and are inherited by the disk, our models suggest that they may be retained in the midplane of the disk. Unfortunately, S_8 does not have any strong infrared active modes and therefore cannot be detected in disks or clouds (Palumbo et al. 1997). We would need observations of other ices in disks to rule out the possibility that S_8 ice is a main carrier.

4.2.2 Implications for Comet Formation

Our results have interesting implications for comets, which form in the midplane of the disk, and are composed of an icy nucleus. Comets are thought to remain largely unprocessed since their formation, which means that their compositions are likely representative of the conditions present in the solar nebula (Calmonte et al. 2016). Several sulfur species have been detected in comets, and sulfur is not observed to be depleted in comets (Calmonte et al. 2016). For example, in the coma of comet 67P/Churyumov-Gerasimenko, the ROSINA instrument (Balsiger et al. 2007) on ESA's Rosetta spacecraft detected H_2S, SO_2, SO, OCS, and H_2CS, as well as several other less abundant sulfur species (Calmonte et al. 2016; Le Roy et al. 2015). H_2S has the highest abundance relative to H_2O at about 1×10^{-2}. SO_2, SO, and OCS are present at abundances of about 1×10^{-3}, and H_2CS has an abundance of about 1×10^{-5}. Calmonte et al. (2016) showed that SO likely originates from the comet's nucleus (as opposed to being processed in the coma).

We can compare our model ice abundances to detections in comets. The diversity of ices produced in our generic model (where sulfur starts as CS and SO) produces high abundances of SO, OCS, and SO_2 ices, but low abundances of H_2S ice. However, in our model in which sulfur initially begins as H_2S, we do get a high abundance of H_2S ice in the lower layers of the disk. This result suggests that the H_2S present in comets was present before the disk formed.

Our models produce a lot of CS ice, which is inconsistent with the nondetection of CS in the coma of 67P Calmonte et al. (2016). One possibility is that the midplane has a much lower C/O ratio than present in our models, as H_2O freezes and settles to the midplane (Hogerheijde et al. 2011; Bergin et al. 2016; Du et al. 2017). We did not model a C/O ratio less than 0.36, but it is likely that the abundance of oxygen in the midplane would lead to higher abundances of oxygen-bearing sulfur species relative to CS ice.

4.2.3 Ice-phase Observations

Sulfur ices have yet to be detected in protoplanetary disks, but OCS ice was detected in a molecular cloud (McClure et al. 2023). Based on our models, future observations of protoplanetary disks targeting OCS, H_2S, SO_2, SO, and CS ices would be most likely to yield detections. These observations would be valuable for determining the initial sulfur form in disks and for connecting the protoplanetary disk phase to cometary abundances.

In several ices, including SO_2, OCS, and H_2CS, we observe that the peak abundance occurs not in the midplane, but at Z/R $\approx$ 0.2 (see Figures 1 and 4). These species have higher binding energies than the main carriers (SO and CS), so they can remain in ice phase higher in the disk. Observations of disks should take into account that absorption from ices such as SO_2, OCS, and H_2CS might not originate in the midplane, where comets and planets are forming, but higher in the disk.

5   Conclusions

We present an updated reaction network for protoplanetary disk chemical modeling that includes several new sulfur species and reactions. We ran a 2D time-dependent disk chemical model to study the main sulfur molecules that form, and we explored the effects of varying the volatile sulfur abundance, C/O ratio, and initial sulfur molecular form.

- The main sulfur carriers are simple molecules like CS, SO, C_2S, SO_2 ice, and OCS ice.

- Gas-phase CS and SO abundances are greatly affected by the C/O ratio. A high C/O ratio is necessary to explain the abundance of CS and lack of SO detections in disks.

- Ice abundances in the lower layers of the disk are greatly influenced by initial sulfur form, while gas-phase molecules in the upper layers of the disk are unaffected by initial sulfur form.

- If we assume that comets undergo little to no chemical processing after formation, then to explain the high abundance of H_2S in comets, there must be some H_2S inherited by the disk.

One of the challenges we had when updating our network were the variations in binding energies reported in the literature, and lack of experiments to determine binding energies for many sulfur species. Experimentally-determined binding energies for sulfur species, such as the sulfur allotropes, would improve our models.

There are many future directions that could be explored with our updated model. For our runs, we focused on a generic disk physical structure. It would be interesting to run the model for different disk structures, such as looking at the effect of central star mass and disk mass on sulfur abundance. One could also study the effects of varied UV fields or X-ray fields. Waggoner and Cleeves (2022) modeled the effects of X-ray flaring events on chemical abundances in disks. They found that X-ray flares caused organosulfides, like C_4S, to increase in abundance. It would be interesting to see if our updated network shows the same build-up of organosulfides in the presence of X-ray flares.

Another future improvement is to vary parameters within a single model run. For example, to match dust ring substructure observed in HD 100546, Keyte et al. (2024) constructed a composite model where the volatile sulfur varies radially by three orders of magnitude. We focused on a generic, gap-free disk, but we could use a similar approach to Keyte et al. (2024) to gain insight on how sulfur chemistry is affected by rings and gaps. Additionally, we used a high C/O ratio throughout the entire disk as a proxy for oxygen settling to the midplane. Future models could

account for settling by varying the C/O ratio vertically within a single run as a more realistic representation of disk processes.

Lastly, one of the big reasons for studying sulfur chemistry in protoplanetary disks is to connect it to exoplanet observations. As large planets form, they heat up the surrounding dust and gas, resulting in local regions in the midplane with higher temperatures. By incorporating local warm spots in the midplane into our models, we could study the sulfur chemistry environments surrounding young planets. These results would give us a glimpse as to how sulfur may have been incorporated into planets in our own solar system, ultimately leading to the emergence of life on Earth.

Acknowledgments

Appendix: Radial Profile of CS and SO Column Densities

Figure 7 shows the radial profiles of the column densities of CS, SO, and C_2S for all model runs, motivated by the observations presented in Le Gal et al. (2021). All three molecules spike in column density close to the star, at radii less than 10 au. The one exception is that CS and C_2S decrease slightly in column density close to the central star in run mid5, where sulfur started as S_8 ice. The disk averaged values are shown in Figure 7 and discussed in Section 4.1.1.

References

Y. Aikawa, G. J. van Zadelhoff, E. F. van Dishoeck, and E. Herbst. Warm molecular layers in protoplanetary disks. A&A, 386:622–632, May 2002. doi: 10.1051/0004-6361:20020037.
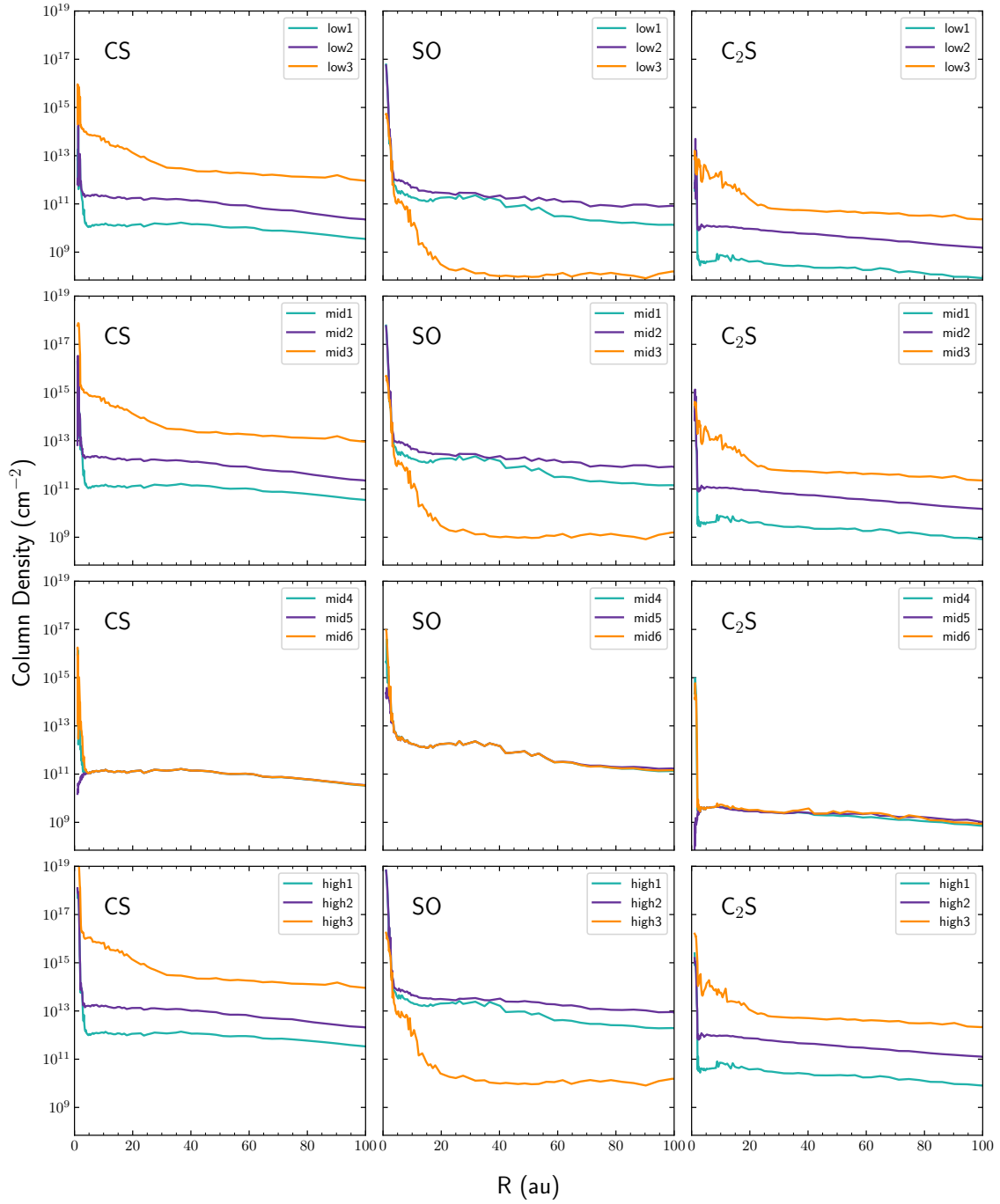
Figure 7: Column density as a function of radius for all model runs. Each column is a different molecule, and each row is a different set of three runs. See Table 1 for the parameters of each run.

D. E. Anderson, G. A. Blake, L. I. Cleeves, E. A. Bergin, K. Zhang, K. R. Schwarz, C. Salyk, and A. D. Bosman. Observing Carbon and Oxygen Carriers in Protoplanetary Disks at Mid-infrared Wavelengths. ApJ, 909(1):55, Mar. 2021. doi: 10.3847/1538-4357/abd9c1.

M. Ansdell, J. P. Williams, N. van der Marel, J. M. Carpenter, G. Guidi, M. Hogerheijde, G. S. Mathews, C. F. Manara, A. Miotello, A. Natta, I. Oliveira, M. Tazzari, L. Testi, E. F. van Dishoeck, and S. E. van Terwisga. ALMA Survey of Lupus Protoplanetary Disks. I. Dust and Gas Masses. ApJ, 828(1):46, Sept. 2016. doi: 10.3847/0004-637X/828/1/46.

M. Asplund, A. M. Amarsi, and N. Grevesse. The chemical make-up of the Sun: A 2020 vision. A&A, 653:A141, Sept. 2021. doi: 10.1051/0004-6361/202140445.

H. Balsiger, K. Altwegg, P. Bochsler, P. Eberhardt, J. Fischer, S. Graf, A. Jäckel, E. Kopp, U. Langer, M. Mildner, J. Müller, T. Riesen, M. Rubin, S. Scherer, P. Wurz, S. Wüthrich, E. Arijs, S. Delanoye, J. de Keyser, E. Neefs, D. Nevejans, H. Rème, C. Aoustin, C. Mazelle, J. L. Médale, J. A. Sauvaud, J. J. Berthelier, J. L. Bertaux, L. Duvet, J. M. Illiano, S. A. Fuselier, A. G. Ghielmetti, T. Magoncelli, E. G. Shelley, A. Korth, K. Heerlein, H. Lauche, S. Livi, A. Loose, U. Mall, B. Wilken, F. Gliem, B. Fiethe, T. I. Gombosi, B. Block, G. R. Carignan, L. A. Fisk, J. H. Waite, D. T. Young, and H. Wollnik. Rosina Rosetta Orbiter Spectrometer for Ion and Neutral Analysis. Space Sci. Rev., 128(1-4):745–801, Feb. 2007. doi: 10.1007/s11214-006-8335-3.

E. A. Bergin and L. I. Cleeves. Chemistry During the Gas-Rich Stage of Planet Formation. In H. J. Deeg and J. A. Belmonte, editors, *Handbook of Exoplanets*, page 137. 2018. doi: 10.1007/978-3-319-55333-7$_1$37.

E. A. Bergin, F. Du, L. I. Cleeves, G. A. Blake, K. Schwarz, R. Visser, and K. Zhang. Hydrocarbon Emission Rings in Protoplanetary Disks Induced by Dust Evolution. ApJ, 831(1):101, Nov. 2016. doi: 10.3847/0004-637X/831/1/101.

T. J. Bethell and E. A. Bergin. The Propagation of Lyα in Evolving Protoplanetary Disks. ApJ, 739(2):78, Oct. 2011a. doi: 10.1088/0004-637X/739/2/78.

T. J. Bethell and E. A. Bergin. Photoelectric Cross-sections of Gas and Dust in Protoplanetary Disks. ApJ, 740(1):7, Oct. 2011b. doi: 10.1088/0004-637X/740/1/7.

A. S. Booth, N. van der Marel, M. Leemker, E. F. van Dishoeck, and S. Ohashi. A major asymmetric ice trap in a planet-forming disk. II. Prominent SO and SO_2 pointing to C/O ¡ 1. A&A, 651:L6, July 2021. doi: 10.1051/0004-6361/202141057.

S. Bruderer. Survival of molecular gas in cavities of transition disks. I. CO. A&A, 559: A46, Nov. 2013. doi: 10.1051/0004-6361/201321171.

U. Calmonte, K. Altwegg, H. Balsiger, J. J. Berthelier, A. Bieler, G. Cessateur, F. Dhooghe, E. F. van Dishoeck, B. Fiethe, S. A. Fuselier, S. Gasc, T. I. Gombosi, M. Hässig, L. Le Roy, M. Rubin, T. Sémon, C. Y. Tzou, and S. F. Wampfler. Sulphur-bearing species in the coma of comet 67P/Churyumov-Gerasimenko. MNRAS, 462: S253–S273, Nov. 2016. doi: 10.1093/mnras/stw2601.

S. Cazaux, H. Carrascosa, G. M. Muñoz Caro, P. Caselli, A. Fuente, D. Navarro-Almaida, and P. Riviére-Marichalar. Photoprocessing of H_2S on dust grains. Building S chains in translucent clouds and comets. A&A, 657:A100, Jan. 2022. doi: 10.1051/0004-6361/202141861.

L. I. Cleeves, E. A. Bergin, C. Qi, F. C. Adams, and K. I. Öberg. Constraining the X-Ray and Cosmic-Ray Ionization Chemistry of the TW Hya Protoplanetary Disk: Evidence for a Sub-interstellar Cosmic-Ray Rate. ApJ, 799(2):204, Feb. 2015. doi: 10.1088/0004-637X/799/2/204.

F. Du, E. A. Bergin, M. Hogerheijde, E. F. van Dishoeck, G. Blake, S. Bruderer, I. Cleeves, C. Dominik, D. Fedele, D. C. Lis, G. Melnick, D. Neufeld, J. Pearson, and U. Yıldız. Survey of Cold Water Lines in Protoplanetary Disks: Indications of Systematic Volatile Depletion. ApJ, 842(2):98, June 2017. doi: 10.3847/1538-4357/aa70ee.

A. Dutrey, S. Guilloteau, and M. Simon. Images of the GG Tauri rotating ring. A&A, 286:149–159, June 1994.

J. K. J. Fogel, T. J. Bethell, E. A. Bergin, N. Calvet, and D. Semenov. Chemistry of a Protoplanetary Disk with Grain Settling and Lyα Radiation. ApJ, 726(1):29, Jan. 2011. doi: 10.1088/0004-637X/726/1/29.

A. Fuente, J. Cernicharo, M. Agúndez, O. Berné, J. R. Goicoechea, T. Alonso-Albi, and N. Marcelino. Molecular content of the circumstellar disk in AB Aurigae. First detection of SO in a circumstellar disk. A&A, 524:A19, Dec. 2010. doi: 10.1051/0004-6361/201014905.

T. J. Harries, J. D. Monnier, N. H. Symington, and R. Kurosawa. Three-dimensional dust radiative-transfer models: the Pinwheel Nebula of WR 104. MNRAS, 350(2): 565–574, May 2004. doi: 10.1111/j.1365-2966.2004.07668.x.

M. R. Hogerheijde, E. A. Bergin, C. Brinch, L. I. Cleeves, J. K. J. Fogel, G. A. Blake, C. Dominik, D. C. Lis, G. Melnick, D. Neufeld, O. Panić, J. C. Pearson, L. Kristensen, U. A. Yıldız, and E. F. van Dishoeck. Detection of the Water Reservoir in a Forming Planetary System. *Science*, 334(6054):338, Oct. 2011. doi: 10.1126/science.1208931.

M. Kama, O. Shorttle, A. S. Jermyn, C. P. Folsom, K. Furuya, E. A. Bergin, C. Walsh, and L. Keller. Abundant Refractory Sulfur in Protoplanetary Disks. ApJ, 885(2): 114, Nov. 2019. doi: 10.3847/1538-4357/ab45f8.

J. F. Kasting, K. J. Zahnle, J. P. Pinto, and A. T. Young. Sulfur, ultraviolet radiation, and the early evolution of life. *Origins of Life and Evolution of the Biosphere*, 19 (3-5):252–253, May 1989. doi: 10.1007/BF02388836.

L. Keyte, M. Kama, A. S. Booth, E. A. Bergin, L. I. Cleeves, E. F. van Dishoeck, M. N. Drozdovskaya, K. Furuya, J. Rawlings, O. Shorttle, and C. Walsh. Azimuthal C/O variations in a planet-forming disk. *Nature Astronomy*, 7:684–693, June 2023. doi: 10.1038/s41550-023-01951-9.

L. Keyte, M. Kama, K.-J. Chuang, L. I. Cleeves, M. N. Drozdovskaya, K. Furuya, J. Rawlings, and O. Shorttle. Spatially resolving the volatile sulfur abundance in the HD 100546 protoplanetary disc. MNRAS, 528(1):388–407, Feb. 2024. doi: 10.1093/mnras/stae019.

J. C. Laas and P. Caselli. Modeling sulfur depletion in interstellar clouds. A&A, 624: A108, Apr. 2019. doi: 10.1051/0004-6361/201834446.

J. A. Lake. Origin of the eukaryotic nucleus determined by rate-invariant analysis of rRNA sequences. Nature, 331(6152):184–186, Jan. 1988. doi: 10.1038/331184a0.

C. J. Law, A. S. Booth, and K. I. Öberg. SO and SiS Emission Tracing an Embedded Planet and Compact ^{12}CO and ^{13}CO Counterparts in the HD 169142 Disk. ApJ, 952 (1):L19, July 2023. doi: 10.3847/2041-8213/acdfd0.

R. Le Gal, K. I. Öberg, R. Teague, R. A. Loomis, C. J. Law, C. Walsh, E. A. Bergin, F. Ménard, D. J. Wilner, S. M. Andrews, Y. Aikawa, A. S. Booth, G. Cataldi, J. B. Bergner, A. D. Bosman, L. I. Cleeves, I. Czekala, K. Furuya, V. V. Guzmán, J. Huang, J. D. Ilee, H. Nomura, C. Qi, K. R. Schwarz, T. Tsukagoshi, Y. Yamato, and K. Zhang. Molecules with ALMA at Planet-forming Scales (MAPS). XII. Inferring the C/O and S/H Ratios in Protoplanetary Disks with Sulfur Molecules. ApJS, 257(1):12, Nov. 2021. doi: 10.3847/1538-4365/ac2583.

L. Le Roy, K. Altwegg, H. Balsiger, J.-J. Berthelier, A. Bieler, C. Briois, U. Calmonte, M. R. Combi, J. De Keyser, F. Dhooghe, B. Fiethe, S. A. Fuselier, S. Gasc, T. I. Gombosi, M. Hässig, A. Jäckel, M. Rubin, and C.-Y. Tzou. Inventory of the volatiles on comet 67P/Churyumov-Gerasimenko from Rosetta/ROSINA. A&A, 583:A1, Nov. 2015. doi: 10.1051/0004-6361/201526450.

N. F. W. Ligterink and M. Minissale. Overview of desorption parameters of volatile and complex organic molecules. A systematic dig through the experimental literature. A&A, 676:A80, Aug. 2023. doi: 10.1051/0004-6361/202346436.

F. Long, G. J. Herczeg, I. Pascucci, E. Drabek-Maunder, S. Mohanty, L. Testi, D. Apai, N. Hendler, T. Henning, C. F. Manara, and G. D. Mulders. An ALMA Survey of CO Isotopologue Emission from Protoplanetary Disks in Chamaeleon I. ApJ, 844(2):99, Aug. 2017. doi: 10.3847/1538-4357/aa78fc.

E. E. Mamajek. Initial Conditions of Planet Formation: Lifetimes of Primordial Disks. In T. Usuda, M. Tamura, and M. Ishii, editors, *Exoplanets and Disks: Their Formation and Diversity*, volume 1158 of *American Institute of Physics Conference Series*, pages 3–10. AIP, Aug. 2009. doi: 10.1063/1.3215910.

M. K. McClure, W. R. M. Rocha, K. M. Pontoppidan, N. Crouzet, L. E. U. Chu, E. Dartois, T. Lamberts, J. A. Noble, Y. J. Pendleton, G. Perotti, D. Qasim, M. G. Rachid, Z. L. Smith, F. Sun, T. L. Beck, A. C. A. Boogert, W. A. Brown, P. Caselli, S. B. Charnley, H. M. Cuppen, H. Dickinson, M. N. Drozdovskaya, E. Egami, J. Erkal, H. Fraser, R. T. Garrod, D. Harsono, S. Ioppolo, I. Jiménez-Serra, M. Jin, J. K. Jørgensen, L. E. Kristensen, D. C. Lis, M. R. S. McCoustra, B. A. McGuire, G. J. Melnick, K. I. Ã-berg, M. E. Palumbo, T. Shimonishi, J. A. Sturm, E. F. van Dishoeck, and H. Linnartz. An Ice Age JWST inventory of dense molecular cloud ices. *Nature Astronomy*, 7:431–443, Apr. 2023. doi: 10.1038/s41550-022-01875-w.

B. A. McGuire. 2021 Census of Interstellar, Circumstellar, Extragalactic, Protoplanetary Disk, and Exoplanetary Molecules. ApJS, 259(2):30, Apr. 2022. doi: 10.3847/1538-4365/ac2a48.

K. I. Öberg, V. V. Guzmán, K. Furuya, C. Qi, Y. Aikawa, S. M. Andrews, R. Loomis, and D. J. Wilner. The comet-like composition of a protoplanetary disk as revealed by complex cyanides. Nature, 520(7546):198–201, Apr. 2015. doi: 10.1038/nature14276.

M. E. Palumbo, T. R. Geballe, and A. G. G. M. Tielens. Solid Carbonyl Sulfide (OCS) in Dense Molecular Clouds. ApJ, 479(2):839–844, Apr. 1997. doi: 10.1086/303905.

N. T. Phuong, A. Dutrey, E. Chapillon, S. Guilloteau, J. Bary, T. L. Beck, A. Coutens, O. Denis-Alpizar, E. Di Folco, P. N. Diep, L. Majumdar, J. P. Melisse, C. W. Lee, V. Pietu, T. Stoecklin, and Y. W. Tang. An unbiased NOEMA 2.6 to 4 mm survey of the GG Tau ring: First detection of CCS in a protoplanetary disk. A&A, 653:L5, Sept. 2021. doi: 10.1051/0004-6361/202141881.

P. Rivière-Marichalar, A. Fuente, G. Esplugues, V. Wakelam, R. le Gal, C. Baruteau, A. Ribas, E. Macías, R. Neri, and D. Navarro-Almaida. AB Aur, a Rosetta stone for studies of planet formation. II. H_2S detection and sulfur budget. A&A, 665:A61, Sept. 2022. doi: 10.1051/0004-6361/202142906.

Z. Rustamkulov, D. K. Sing, S. Mukherjee, E. M. May, J. Kirk, E. Schlawin, M. R. Line, C. Piaulet, A. L. Carter, N. E. Batalha, J. M. Goyal, M. López-Morales, J. D. Lothringer, R. J. MacDonald, S. E. Moran, K. B. Stevenson, H. R. Wakeford, N. Espinoza, J. L. Bean, N. M. Batalha, B. Benneke, Z. K. Berta-Thompson, I. J. M. Crossfield, P. Gao, L. Kreidberg, D. K. Powell, P. E. Cubillos, N. P. Gibson, J. Leconte, K. Molaverdikhani, N. K. Nikolov, V. Parmentier, P. Roy, J. Taylor, J. D. Turner, P. J. Wheatley, K. Aggarwal, E. Ahrer, M. K. Alam, L. Alderson, N. H. Allen, A. Banerjee, S. Barat, D. Barrado, J. K. Barstow, T. J. Bell, J. Blecic, J. Brande,

S. Casewell, Q. Changeat, K. L. Chubb, N. Crouzet, T. Daylan, L. Decin, J. Désert, T. Mikal-Evans, A. D. Feinstein, L. Flagg, J. J. Fortney, J. Harrington, K. Heng, Y. Hong, R. Hu, N. Iro, T. Kataria, E. M. R. Kempton, J. Krick, M. Lendl, J. Lillo-Box, A. Louca, J. Lustig-Yaeger, L. Mancini, M. Mansfield, N. J. Mayne, Y. Miguel, G. Morello, K. Ohno, E. Palle, D. J. M. Petit dit de la Roche, B. V. Rackham, M. Radica, L. Ramos-Rosado, S. Redfield, L. K. Rogers, E. L. Shkolnik, J. Southworth, J. Teske, P. Tremblin, G. S. Tucker, O. Venot, W. C. Waalkes, L. Welbanks, X. Zhang, and S. Zieba. Early Release Science of the exoplanet WASP-39b with JWST NIRSpec PRISM. Nature, 614(7949):659–663, Feb. 2023. doi: 10.1038/s41586-022-05677-y.

D. Semenov, C. Favre, D. Fedele, S. Guilloteau, R. Teague, T. Henning, A. Dutrey, E. Chapillon, F. Hersant, and V. Piétu. Chemistry in disks. XI. Sulfur-bearing species as tracers of protoplanetary disk physics and chemistry: the DM Tau case. A&A, 617:A28, Sept. 2018. doi: 10.1051/0004-6361/201832980.

C. N. Shingledecker, T. Lamberts, J. C. Laas, A. Vasyunin, E. Herbst, J. Kästner, and P. Caselli. Efficient Production of S_8 in Interstellar Ices: The Effects of Cosmic-Ray-driven Radiation Chemistry and Nondiffusive Bulk Reactions. ApJ, 888(1):52, Jan. 2020. doi: 10.3847/1538-4357/ab5360.

I. W. M. Smith, E. Herbst, and Q. Chang. Rapid neutral-neutral reactions at low temperatures: a new network and first results for TMC-1. MNRAS, 350(1):323–330, May 2004. doi: 10.1111/j.1365-2966.2004.07656.x.

K. M. Strom, S. E. Strom, S. Edwards, S. Cabrit, and M. F. Skrutskie. Circumstellar Material Associated with Solar-Type Pre-Main-Sequence Stars: A Possible Constraint on the Timescale for Planet Building. AJ, 97:1451, May 1989. doi: 10.1086/115085.

O. Tange. Gnu parallel 20240122 ('frederik x'), Jan. 2024. URL https://doi.org/10.5281/zenodo.10558745.

R. Teague, T. Henning, S. Guilloteau, E. A. Bergin, D. Semenov, A. Dutrey, M. Flock, U. Gorti, and T. Birnstiel. Temperature, Mass, and Turbulence: A Spatially Resolved Multiband Non-LTE Analysis of CS in TW Hya. ApJ, 864(2):133, Sept. 2018. doi: 10.3847/1538-4357/aad80e.

A. R. Waggoner and L. I. Cleeves. Classification of X-Ray Flare-driven Chemical Variability in Protoplanetary Disks. ApJ, 928(1):46, Mar. 2022. doi: 10.3847/1538-4357/ac549f.

C. Walsh, R. A. Loomis, K. I. Öberg, M. Kama, M. L. R. van 't Hoff, T. J. Millar, Y. Aikawa, E. Herbst, S. L. Widicus Weaver, and H. Nomura. First Detection of Gas-phase Methanol in a Protoplanetary Disk. ApJ, 823(1):L10, May 2016. doi: 10.3847/2041-8205/823/1/L10.

B. J. Williams, L. I. Cleeves, C. Eistrup, and J. P. Ramsey. Deep Search for Molecular Oxygen in TW Hya. ApJ, 956(2):135, Oct. 2023. doi: 10.3847/1538-4357/acf717.

J. P. Williams and L. A. Cieza. Protoplanetary Disks and Their Evolution. ARA&A, 49(1):67–117, Sept. 2011. doi: 10.1146/annurev-astro-081710-102548.

M. C. Wyatt. Evolution of debris disks. ARA&A, 46:339–383, Sept. 2008. doi: 10.1146/annurev.astro.45.051806.110525.